RUSSIAN JOURNAL OF NONDESTRUCTIVE TESTING, 2025, No. 1, pp. 14–26

ACOUSTIC METHODS

IDENTIFICATION OF DIFFUSION INTERLAYERS OF DISSIMILAR WELDS OF STEEL 20 AND STEEL 12KH18N10T UNDER STATIC TENSION BY ACOUSTIC EMISSION METHOD

© 2025 V. A. Barat[a,b,*], A. Yu. Marchenkov[a,**], S. V. Ushanov[a], E. A. Lepsheev[a,b], G. B. Sviridov[a], N. V. Lavrik[a], and S. V. Elizarov[b]

[a]*NRU MPEI, Moscow, Russia*
[b]*LLC "INTERUNIS-IT", Moscow, Russia*
**e-mail: BaratVA@mpei.ru*
***MarchenkovAY@mpei.ru*

Received August 09, 2024
Revised November 05, 2024
Accepted November 08, 2024

Abstract. The paper investigates the possibility of detecting specific structural defects of dissimilar welded joints using the acoustic emission (AE) method — carbide and decarburized ferrite interlayers in dissimilar welded joints of 12Kh18N10T austenitic and 20 pearlitic steels, formed during welding and subsequent operation. Detection is carried out based on the analysis and comparison of AE data flow parameters and spectral characteristics of signals obtained during testing of defect-free welded joints and welded joints with diffusion interlayers of various thicknesses.

Keywords: *acoustic emission, dissimilar welds, diffusion interlayers*

DOI: 10.31857/S01303082250102e7

1. INTRODUCTION

Modern trends in the improvement of industrial products and structures lead to increased requirements to the used structural materials and technologies of their processing. In particular, combined structures obtained by welding of dissimilar or clad materials are becoming more and more widely used. They are used when the operating conditions of individual parts of the structure differ in terms of temperature, aggressiveness of the environment or special mechanical effects such as wear and tear or alternating loads.

During welding, heat treatment or high-temperature operation of dissimilar welded joints in the zones of fusion and thermal influence, layers may be formed due to crystallization processes or diffusion redistribution of chemical elements included in the composition of welded and filler materials. In the case of fusion welding of dissimilar steels, the formation of diffusion interlayers is mostly associated with the migration of carbon, which forms solid solutions of introduction with iron [1]. If the welded joint is formed by steels of different alloying, then in the fusion zone, the processes of diffusion redistribution of predominantly carbon will occur due to its high diffusion mobility. With increasing temperature and time of stay of welded joints at high temperatures, these processes occur even more intensively, so in welded joints of dissimilar steels, decarburized interlayers and layers with increased carbide content are often observed on different sides of the fusion line [2]. The size of such interlayers is largely determined by the welding method and operating conditions of the welded joint, on which the intensity of physical processes occurring at the interface between solid and liquid phases depends [3].

The formation of diffusion interlayers is a fairly common process characteristic of welding dissimilar materials or homogeneous composite materials, for example, when welding clad steels [4].

Diffusion interlayers can be formed not only in welded joints obtained by fusion, but also by pressure welding. Namely, the works [5, 6] describe cases of formation of diffusion interlayers in layered intermetallic composites obtained by explosion welding. Diffusion interlayers are

formed at the stage of heat treatment, and their thickness depends on the temperature and duration of the process. The formation of diffusion interlayers is observed during vacuum welding of powder materials [7], as well as during sintering of steel base with powder mixtures forming a protective coating [8].

Diffusion interlayers can be considered a defect in the structure of the welded joint, since their formation can cause premature failure of the product under conditions of operation at high temperatures [1]. In addition, under certain chemical and structural-phase composition of welded metals, conditions for the formation of brittle interlayers and the development of cracks in the weld zone can be created [9].

Identification of diffusion interlayers is usually carried out by means of labor-intensive metallographic studies of etched microslides, allowing to clarify the structure and thickness of diffusion interlayers, as well as the use of scanning electron microscopy and energy dispersive X-ray spectroscopy to clarify the chemical composition of the formed diffusion zones. To estimate the local mechanical properties in the zone of diffusion interlayers, the techniques of scribing and indentation [10] are used, in which the values of the strength and yield strength in the investigated zone are determined indirectly by the values of the metal hardness characteristics.

It is difficult to detect diffusion interlayers using physical inspection methods, since they do not differ in density, electrical conductivity and acoustic impedance from the material of the welded joint and periweld zone. An exception is the method of acoustic emission (AE), which, due to its sensitivity to changes in the structural parameters of the controlled materials, makes it possible to detect not only continuity defects, but also structural defects. In particular, the authors of this article have conducted preliminary studies confirming the possibility of detecting diffusion layers in combined welded joints by AE method [1].

Within the framework of this work, the AE patterns at static stretching of samples of dissimilar welded joints of steel 20 and 12Kh18N10T were investigated. Defect-free welded joints (i.e. without diffusion interlayers) and welded joints with diffusion interlayers of different thicknesses obtained by argon-arc welding (TIG) were considered. On the basis of analysis of AE data flow parameters, taking into account the nature of the frequency spectrum, the patterns corresponding to the presence of diffusion interlayers in the structure of a dissimilar welded joint were revealed.

2. RESEARCH MATERIALS AND METHODS

The objects of research in this work were dissimilar butt welded joints of steel 20 (carbon steel with ferrite-perlite structure) and steel 12Kh18N10T (alloy steel of austenitic class). To make the welded joints, 3 mm thick sheets were used, which were cut into strips of 1000 mm long and 200 mm wide and welded together using argon-arc welding. Argon-arc welding was butt welded on both sides, Sabaros O101 wire with austenitic structure was selected as a filler material. The chemical composition of the filler wire is given in Table 1. The use of Sabaros O101 wire allows to obtain austenitic structure of weld metal, which is optimal in terms of its mechanical and operational properties.

Table 1. Chemical composition of Sabaros O101 filler wire, % wt %

C	Si	Cr	Ni	Mn	Fe
0,10	0,50	19,0	9,0	6,0	Basis

Manufacturing of specimens for mechanical tests was carried out by cutting welded sheets using laser cutting. The shape and dimensions of the test specimen were selected taking into account the recommendations of normative documents, as well as taking into account the peculiarities of the tests. The width of the working part of the specimen was chosen to be 20 mm in order to be able to reliably install an acoustic emission transducer with a diameter of 15 mm on its surface. The weld seam on the specimen was located in the middle of the working part. The width of the gripping part of the specimens was chosen to be 50 mm in order to avoid plastic deformation

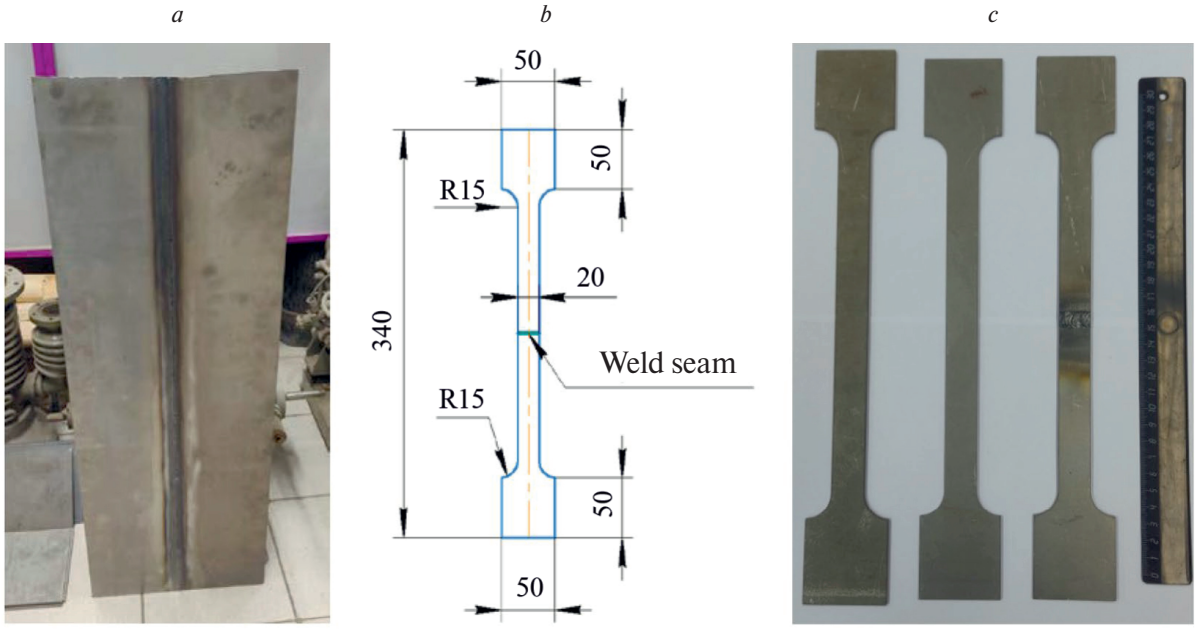

Fig. 1. Welded sheets from 20 and 12Kh18N10T steels (*a*); diagram of a tensile test specimen (*b*); photographs of some fabricated specimens for mechanical tests (*c*).

of 12Kh18N10T steel in the gripping part during testing. The scheme and photos of the specimens are shown in Fig. 1.

In order to form diffusion interlayers in welded joints, inherent in dissimilar welded joints operating for a long time at high temperatures, some of the fabricated welded specimens were subjected to subsequent heat treatment (HT), simulating long-term operation of these welded joints at high temperatures.

Heat treatment was carried out in Nabertherm P180 furnace at 650°C with different holding times at maximum temperature (for 1 h; 5 h; 25 h) to form layers of different thicknesses. Then, using optical microscopy on a Zeiss Observer Z1m microscope, the microstructure of the weld zone of welded joints was studied and the thicknesses of carbide and decarburized interlayers were measured (Fig. 2). The average values of the thicknesses of diffusion layers are shown in Table 2, from which it can be seen that the increase in holding time leads to intensification of the process of carbon diffusion from steel 20 into the weld metal, resulting in an increase in the thicknesses of diffusion layers.

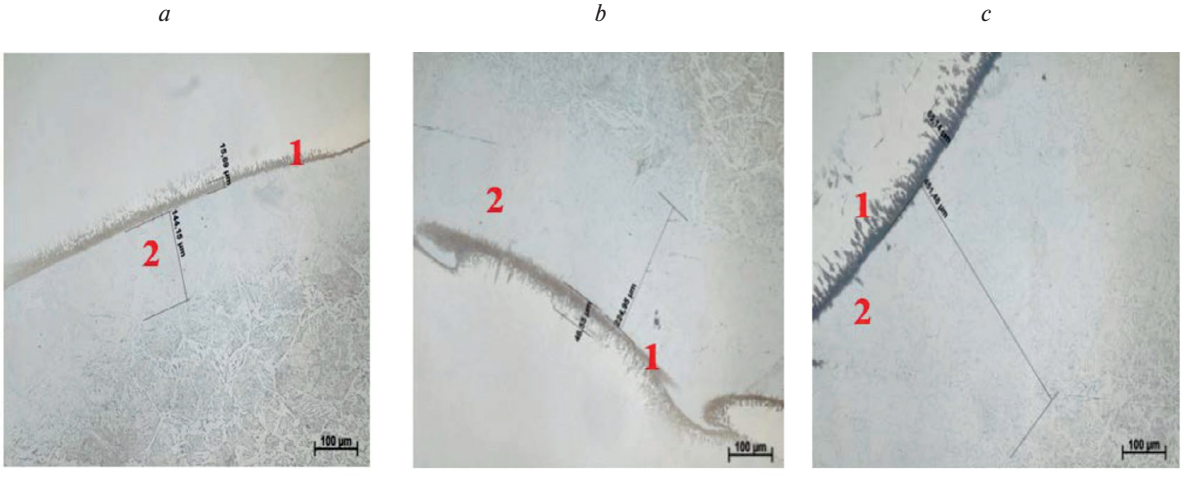

Fig. 2. Photographs of the fusion line on the side of steel 20 with measured values of thicknesses of diffusion layers (carbide and decarburized) after heat treatment at 650°C with 1 h (*a*); 5 h (*b*); 25 h (*c*): 1 – carbide interlayer; 2 – decarburized interlayer. Magnification 200×.

Table 2. Average values of thickness of diffusion interlayers in welded joints of steel 20 with steel 12Kh18N10T, obtained by Argon-arc welding, after heat treatment

No. of the regime	Soaking time at high temperature, h	Thickness of decarburized layer, μm	Carbide interlayer thickness, μm
1	1	145	20
2	5	225	45
3	25	600	65

Fig. 3 shows a photograph of the fusion line from the side of steel 20, the carbon distribution in this area and the chemical composition of the carbide interlayer obtained by scanning electron microscopy (SEM) and energy dispersive X-ray spectroscopy (EDS) on a Tescan Mira 3 microscope. The studies carried out using EDS allowed to establish that the carbide layer in the welded joint under study consists mainly of chromium carbides.

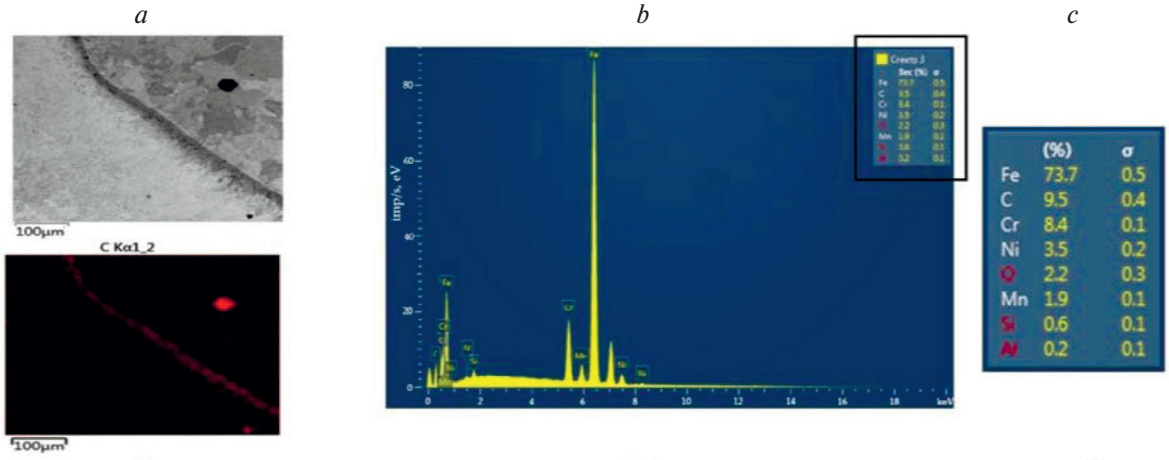

Fig. 3. Photograph of the welded joint area near the fusion line on the steel 20 side (*a*); carbon distribution in this area (*b*); results of chemical composition determination in the carbide interlayer (*c*).

Static tensile tests were performed on an Instron 5982 machine with a constant strain rate of 0.5 mm/min. The low strain rate was chosen in order to reveal the patterns of AE generation at different stages of deformation of the samples. The photos of the experiment are shown in Fig. 4.

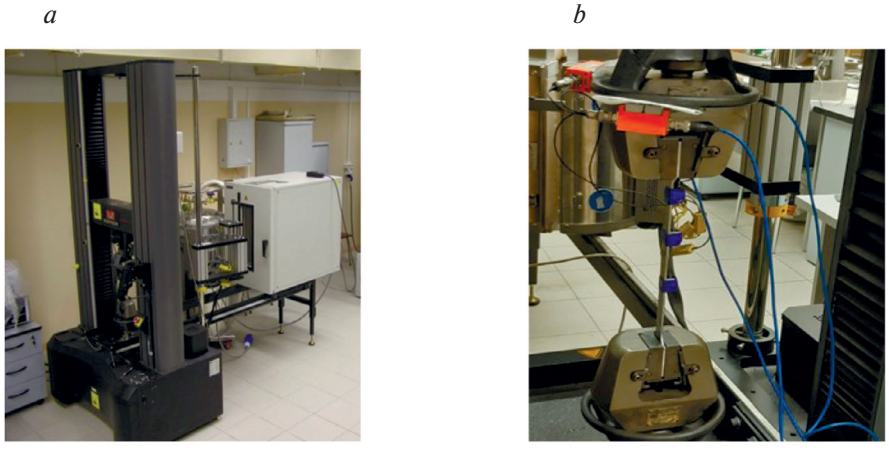

Fig. 4. Instron 5982 universal testing machine (*a*) and photo of the specimen in the grips with AE sensors attached (*b*).

The specimens were tested before rupture with synchronous recording of AE signals during the test. For this purpose, four AE transducers were fixed on the specimen, two of them were located in the vicinity of the specimen center, and the other two – in the area of the grips (Fig. 4*b*). Such a scheme with the use of additional AE transducers makes it possible to eliminate acoustic interference associated with the influence of the grips of the testing machine.

To exclude the influence of interference associated with the loading of the sample, transducers with a sensitivity variation of no more than ±0.5 dB were selected. The data were then pre-processed by selecting for analysis only those acoustic events that had both maximum amplitudes and minimum recording times observed on the measurement channels that were installed in close proximity to the welded joint.

AE data were recorded using the A-Line 32 system (LLC "INTERUNIS-IT", Russia) with PAEF-014 preamplifiers and GT200 AE transducers (LLC "Global Test", Russia) with a resonance frequency of 180 kHz. To suppress the noise of the test machine during data acquisition, a digital filter with a bandwidth of 100–400 kHz shifted to the high frequency region was used. The amplitude discrimination threshold was 40 dB.

To determine the mechanical properties of the materials to be welded in the initial state, separate tensile tests were performed on specimens of base metal (steel 20 and steel 12X18N10T) of identical geometry.

In addition, to assess possible changes in the mechanical properties of steels during high-temperature heat treatment, tensile tests were performed on samples from steel 20 and samples from steel 12Kh18N10T after heat treatment. To evaluate the changes in the microstructure of these steels after heat treatment, metallographic analysis was carried out using optical microscopy.

3. RESULTS

3.1 Results of tensile testing of specimens and microstructure studies

The results of tensile tests on specimens cut from the base metal are presented in Table 3.

Table 3. Mechanical properties of 20 and 12Kh18N10T steel specimens determined by tensile testing (average values)

Material / heat treatment mode	Yield strength σ_t or $\sigma_{0,2}$, MPa	Tensile strength σ_c, MPa	Ultimate uniform elongation δ_{ra}, %	Relative elongation after rupture δ_k, %
Steel 20				
In the state of delivery	321	398	15	17
After treatment 650°C, 1 h	320	395	18	21
After treatment 650°C, 5 h	313	384	19	22
After treatment 650°C, 25 h	307	369	19	21
12Kh18N10T steel				
In the state of delivery	270	631	55	58
After treatment 650°C, 25 h	265	625	57	61

Typical tensile diagrams for 12Kh18N10T steel and 20 steel specimens are shown in Fig. 5*a, b,* respectively. From the diagrams and the table we can see that steel 12Kh18N10T and steel 20 in the initial state have close values of yield strength – in steel 12Kh18N10T the value of conditional yield strength is $\sigma_{0,2} \approx 270$ MPa, in steel 20 there is a yield point with an average

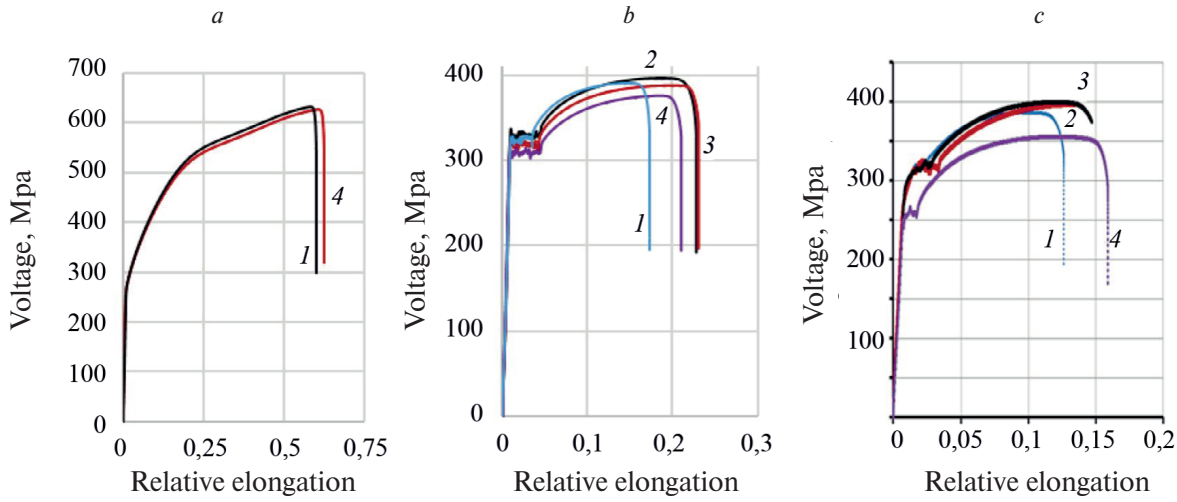

Fig. 5. Tensile diagrams of specimens made of 12Kh18N10T steel (*a*); steel 20 (*b*) and dissimilar welded joint (*c*): *1* – without heat treatment; *2* – after 1 h heat treatment at 650°C; *3* – after 5 h heat treatment at 650°C; *4* – after 25 h heat treatment at 650°C at 650°C.

stress $\sigma_t \approx 320$ MPa. Thus, steel 12Kh18N10T is characterized by higher values of tensile strength and plasticity characteristics.

From Fig. 5*a* and Table 3 it follows that heat treatment has no effect on the mechanical properties of steel 12Kh18N10T – characteristics of strength and plasticity of steel before and after processing are practically the same. Microstructure studies also revealed no changes after heat treatment (Fig. 6).

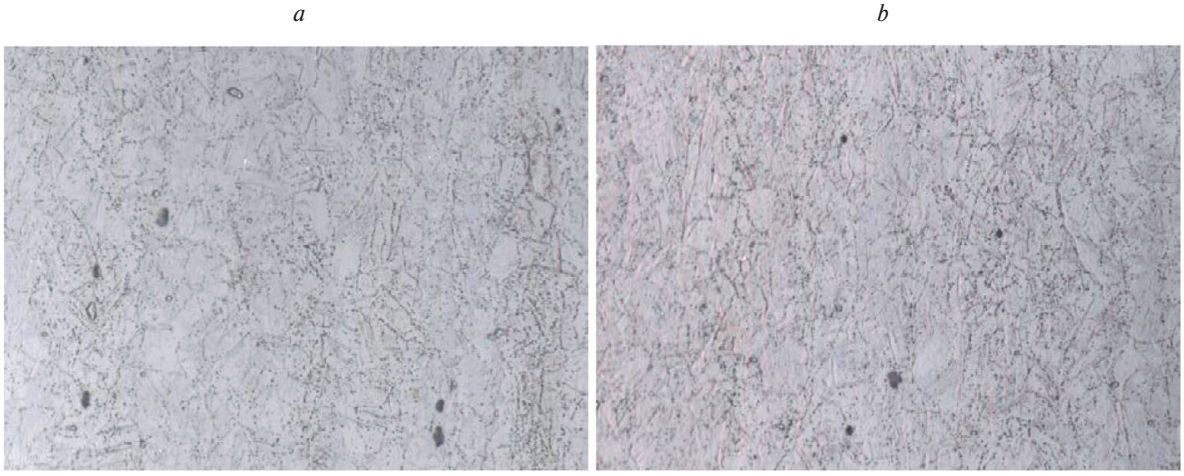

Fig. 6. Microstructure of 12Kh18N10T steel in the initial state (*a*) and after heat treatment at 650°C, 25 h (*b*).

Steel 20 after heat treatment undergoes some changes in mechanical properties, consisting in a slight increase in ductility and a decrease in yield strength with increasing time exposure at high temperature (see Table 3 and Fig. 5*b*). Changes are observed in the microstructure of steel 20 after heat treatment. Fig. 7 shows photographs of the microstructure of steel 20 in the initial state and after heat treatment with maximum time exposure (25 h). It can be seen from the photographs that heat treatment leads to gradual dissociation of cementite, which is reflected in the mechanical characteristics of the steel under study.

The tensile diagram of specimens with welded joints (Fig. 5*c*) shows several characteristic deformation sections. For the specimen without heat treatment (see Fig. 5*c*, diagram *1*), up to a stress of about 250 MPa, a section of elastic deformation is observed – both

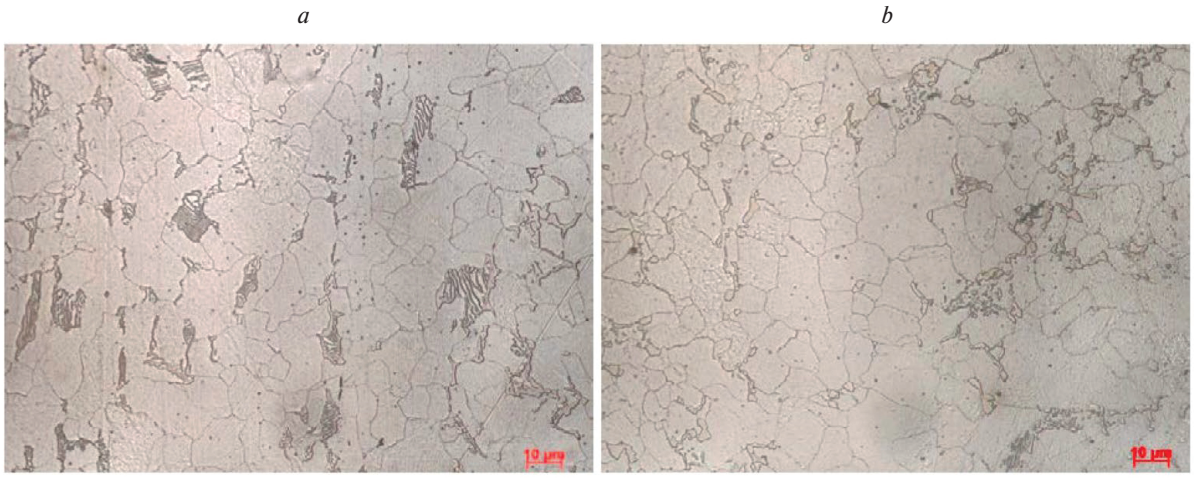

Fig. 7. Microstructure of steel 20 in the initial state (*a*) and after heat treatment at 650°C, 25 h (*b*); magnification 1000×.

steels and the welded seam deform elastically. At a stress of about 250 MPa, plastic deformation of 12Kh18N10T steel begins, at a stress of ≈ 320 MPa, a yield point from steel 20 is observed in the diagram. The yield area is followed by a developed section of strain hardening, where both steels deform elasto-plastically. After reaching the stress maximum, a decline is observed in the diagram, after which the specimen fails along the base metal on the steel 20 side.

After heat treatment the properties of welded joints underwent some changes. Tensile diagrams of welded specimens after different heat treatment modes are presented in Fig. 5*c* (diagrams *2–4*). The diagrams show that during heat treatment under the regimes (650°C, 1 h) and (650°C, 5 h) the strength characteristics of the welded specimens remained at the same level, while there was an increase in the plasticity of the metal. At longer high-temperature exposure (650°C, 25 h) there was a decrease in the level of tensile strength and yield strength of the welded joint due to a decrease in the corresponding characteristics of steel 20. Failure of all specimens also occurred along the base metal on the side of steel 20.

3.2 Analysis of AE data

Fig. 8 shows the data of AE activity and amplitudes of AE pulses obtained for a defect-free sample of a dissimilar welded joint (Fig. 8*a*), a sample with small thickness layers up to 145 μm (Fig. 8*6*) and a sample with medium thickness layers up to 225 μm (Fig. 8*c*). The general patterns of AE data for the defect-free specimen and for specimens with diffusion interlayers

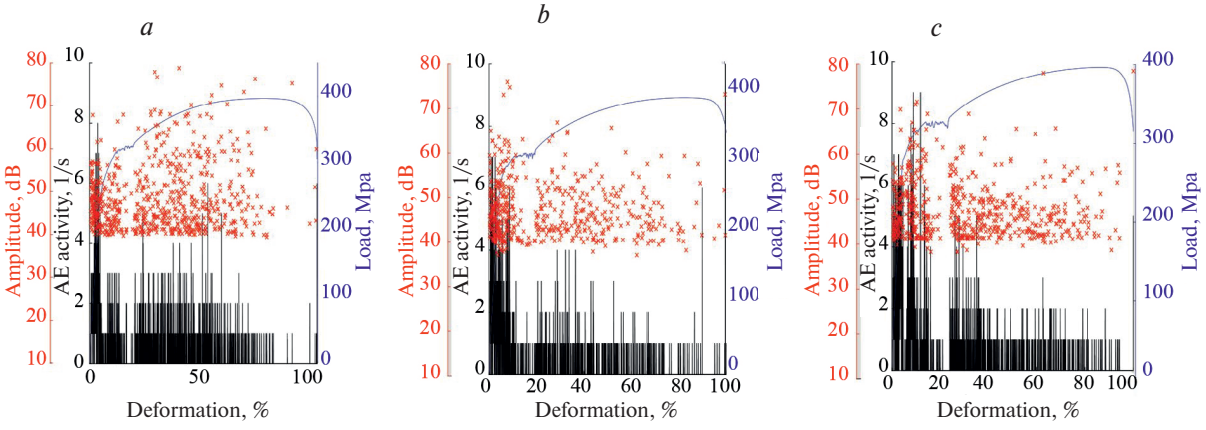

Fig. 8. Time dependence of pulse amplitudes and AE activity for a defect-free welded joint (*a*); for a welded joint with diffusion interlayers up to 145 μm (*b*) and with diffusion interlayers up to 225 μm (*c*).

are generally similar – at the elastic deformation site and at the initial stage of strain hardening there is an increase in AE activity, then a pronounced acoustic quiescence during the period of passing the yield point and a repeated increase in the level of AE activity at the strain hardening site. The presence of AE activity in the elastic deformation region of steel 20 is an atypical phenomenon, since there are no AE sources associated with dislocation motion in the elastic region. The authors [11, 12] hypothesized the influence of magnetomechanical processes occurring during deformation on the AE data. In the process of elastic deformation of a ferromagnetic material, there is a magnetoelastic effect, which consists in the fact that a monotonous smooth change in mechanical stress leads to a jump-like change in the magnetic field strength, which in turn leads to the displacement of domain walls – the boundaries between magnetic domains with different magnetization direction [13, 14]. The acoustic quiescence during the time period corresponding to the yield point is explained by the fact that the amplitude of AE sources associated with dislocation processes at this stage of loading is below the established threshold of amplitude discrimination.

However, in the local section at a stress of 300 MPa, corresponding to the strength limit of the ferrite phase, the level of AE activity and amplitudes of AE pulses for specimens with diffusion interlayers is higher than for a defect-free specimen. This effect is not too obvious on time dependences, because at constant strain rate the stress growth from 290 to 310 MPa occurs in 1–2 min, while the total time from the beginning of loading to failure of the specimen is more than 1 h.

For more detailed analysis of AE data parameters at different stress levels, the time dependences presented in Fig. 8 were transformed into dependences of AE pulse amplitudes and activity on mechanical stress values. Fig. 9 shows the dependences of AE activity and average amplitude of AE pulses on the value of mechanical stress at the elastic deformation section (up to 320 MPa). The values of AE-parameters presented in Fig. 9 were obtained as a result of nonlinear transformation of the abscissa axis, since the growth of mechanical stress by 1 MPa at different stages of loading occurs for different time intervals. Such a way of presentation of diagnostic data allows for a more detailed analysis of the nature of changes in AE-parameters in the elastic deformation section of the tensile diagram. However, it should be noted that the AE-activity parameter calculated with respect to the mechanical stress value is modified with respect to the classical definition in accordance with GOST 27655-88.

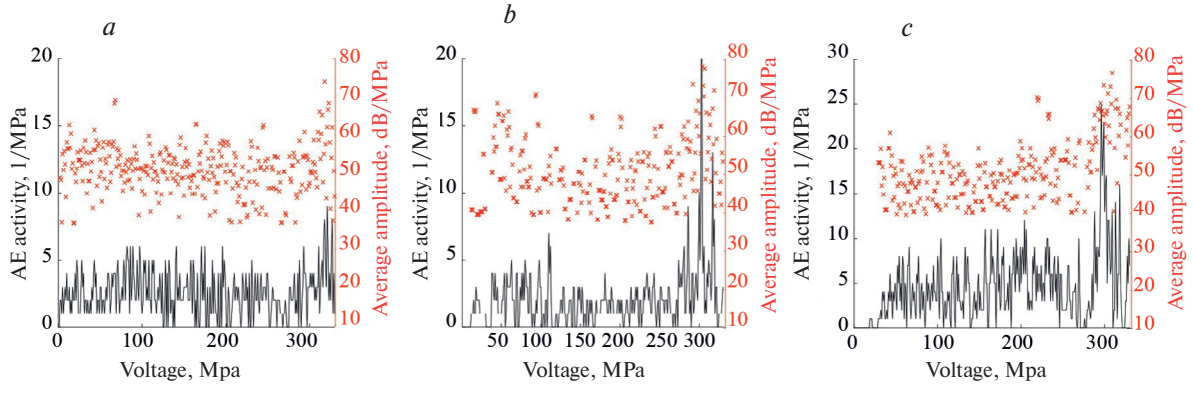

Fig. 9. Voltage dependence of pulse amplitudes and AE activity for a defect-free welded joint in the elastic strain region (*a*); for a welded joint with diffusion interlayers up to 145 μm (*b*) and with diffusion interlayers up to 225 μm (*c*).

Analysis of the data presented in Fig. 9 shows that in the case of samples with diffusion interlayers, there is a pronounced local increase in the values of AE pulse amplitudes and the level of AE activity at a stress of 300 MPa, corresponding to the strength limit of the ferrite phase.

For the samples that have undergone long-term heat treatment (exposure at 650°C for 25 h), the character of AE data differs from the previous cases – in the section of strain hardening

lower values of AE activity are registered than for samples with shorter heat treatment time, and the values of amplitudes of AE impulses are 10–15 dB higher than in the previous cases (Fig. 10). Such a change in the character of AE data can be explained by the fact that as a result of prolonged heat treatment in steel 20 there were structural changes associated with the removal of internal stresses, which led to a decrease in AE activity. Also, as a result of long-term heat treatment, there was an increase in the average grain size of ferrite in the base metal structure, which led to an increase in the amplitudes of AE pulses.

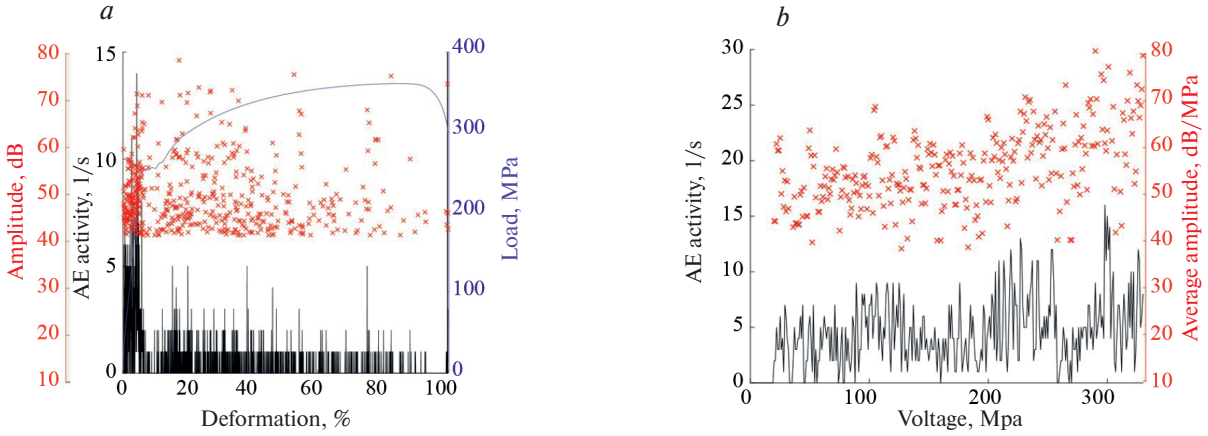

Fig. 10. AE data for a sample of a dissimilar welded joint with diffusion layers up to 600 μm thick: dependences of amplitude pulses and AE activity on time (*a*) and on voltage (*b*).

The growth of AE-activity and the level of amplitudes of AE pulses at a stress of 300 MPa, close to the strength limit of the ferrite phase, is not as pronounced as for samples with diffusion interlayers of smaller thickness. Presumably, this may be due to a decrease in the effect of contact hardening of the soft interlayer due to an increase in the width of the ferrite interlayer in samples after prolonged heat treatment [2, 16].

Since heat treatment changes not only the microstructure of a dissimilar welded joint, but also the microstructure of steel 20, it is necessary to exclude the influence of the base metal deformation on the AE parameters in the stress range of 290–310 MPa to substantiate the reliability of the obtained results. For this purpose, tensile experiments were carried out on steel 20 specimens in the initial state and after heat treatment.

Fig. 11 shows the dependences of AE pulse amplitudes and AE activity on voltage. As can be seen from the figures, the AE-parameters for steel 20 in the initial state and after heat treatment change stationary, local increase of activity and amplitudes of AE pulses in the region of 300 MPa is not observed.

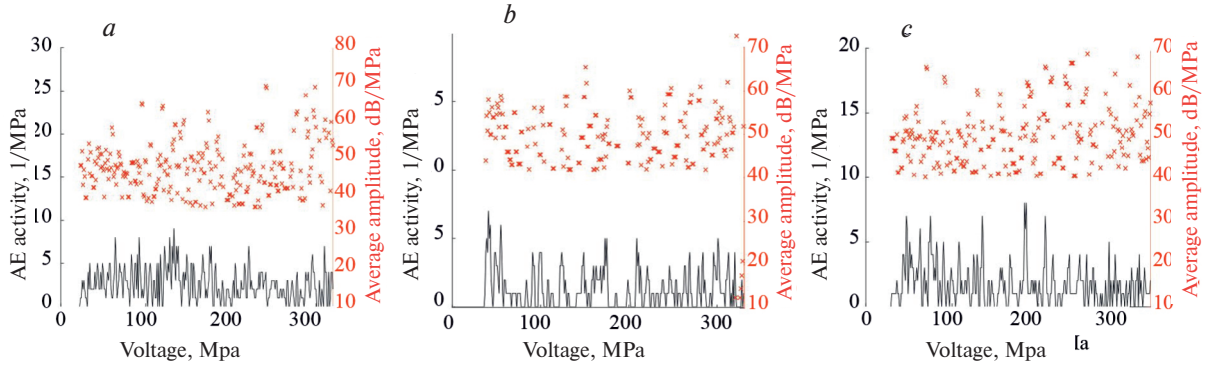

Fig. 11. Dependence of pulse amplitudes and AE activity on tensile stress of steel 20 specimens in the delivery state (*a*) after 5 h of treatment at 650°C (*b*); after 25 h of treatment at 650°C (*c*).

3.3 Study of the spectrum of AE-signals

For more detailed analysis of AE data, the spectra of AE signals recorded at stresses in the region of ferrite phase tensile strength values – from 290 to 310 MPa – were analyzed.

Fig. 12 shows characteristic spectra of AE-signals obtained during testing of a defect-free specimen (Fig. 12*a*) and specimens with diffusion interlayers of different thicknesses. Fig. 12*b* corresponds to the minimum thickness of diffusion interlayers, Fig. 12*c* – to the maximum. In spite of the fact that the GT200 resonance transducer is used for measurements, its high sensitivity in the frequency range of 100–300 kHz allowed us to reveal changes in the parameters of the frequency spectrum of AE signals in samples with diffusion layers. The spectrum of signals obtained during testing of defect-free specimens is narrow-band, with a maximum in the area of the resonant frequency of the transducer. When testing specimens with diffusion layers, more broadband signals appear, and the greater the width of the diffusion layer, the wider the spectrum of the AE signal.

To characterize the spectra of AE signals, the median frequency f_{med}, corresponding to the center of the mass spectrum, is traditionally used [17]:

$$\int_{f_l}^{f_{med}} S(f)df = \int_{f_{med}}^{f_u} S(f)df, \quad (1)$$

where $S(f)$ is the spectrum of the signal; f_l and f_u are the lower and upper frequency of the spectrum, respectively.

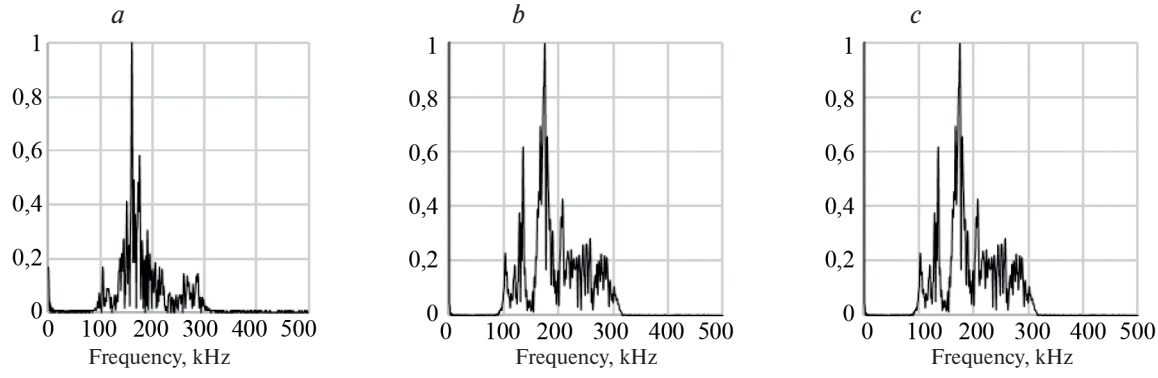

Fig. 12. Characteristic spectra of AE-signals obtained during testing of samples of dissimilar welded joints: defect-free sample (*a*); sample with interlayers up to 145 μm (*b*); sample with interlayers up to 600 μm (*c*).

The median frequency is an integral parameter that allows us to estimate the overall change in the signal spectrum: the shift of energy to the low-frequency or high-frequency region. Fig. 13 shows the empirical distributions of the median frequency of the spectra calculated from samples of signals recorded at stresses of 290–310 MPa for defect-free specimens (Fig. 13*a*) and for specimens with diffusion layers of different thickness (Fig. 13*b*). For defect-free specimens, the characteristic median frequency is in the region of 165 kHz, while for specimens with diffusion interlayer, the median frequency shifts to the right and localizes in the region of 180 kHz. It should also be noted that when testing specimens with diffusion layers, signals with median frequency value more than 200 kHz are registered, while for defect-free specimens signals with such parameter values are not registered.

Another informative parameter that allows us to identify differences in the AE data obtained for defective and defect-free samples is the entropy of the spectrum *E:*

$$E = -\sum_{f=f_l}^{f_u} PSD(f)\log_2\left[PSD(f)\right], \quad (2)$$

where $PSD(f)$ is the power spectral density.

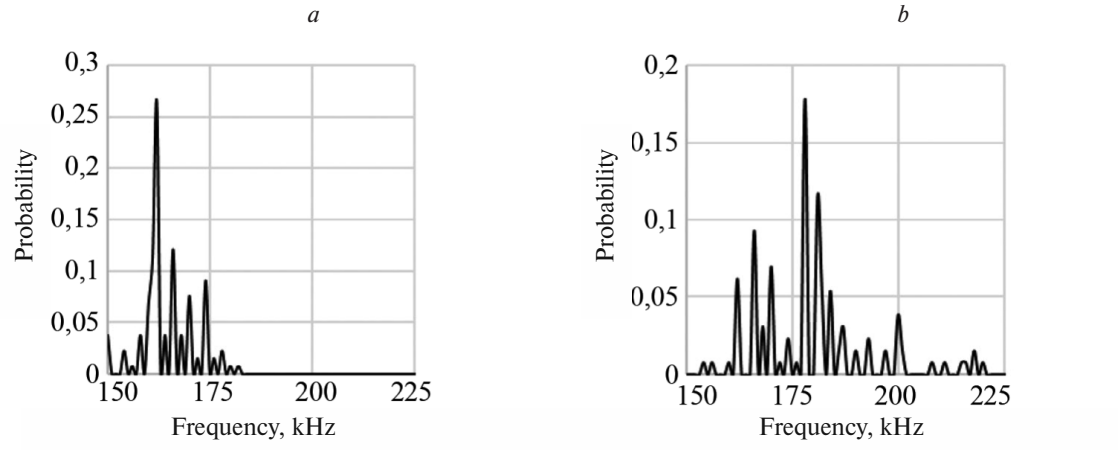

Fig. 13. Empirical distributions of median frequency for defect-free samples (*a*); for samples with diffusion interlayers (*b*).

The spectra of AE signals obtained during testing of defect-free specimens are narrow-band, in the presence of diffusion interlayers a significant fraction of AE signals acquires a broader-band spectrum, with such transformation the entropy of the spectra increases.

Fig. 14 shows the spectral entropy distributions for the AE signals obtained during testing of defect-free specimens (Fig. 14*a*) and during testing of specimens with diffusion interlayers of different thickness (Fig. 14*b*). As can be seen from the figure, the distribution of spectral entropy corresponding to the defect-free specimen and the specimen with diffusion interlayers is the same as that of the diffusion interlayers.

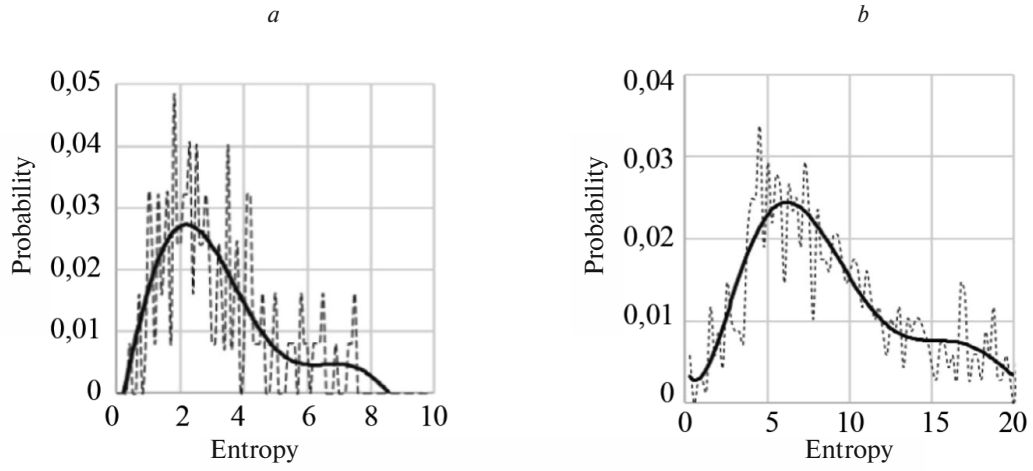

Fig. 14. Distribution of the entropy of the spectrum obtained for the test data of defect-free specimens (*a*); specimens with diffusion layers (*b*).

The mean and variance of the spectral entropy are significantly different: the mean and variance of the spectral entropy are higher for the data corresponding to the test of specimens with diffusion layers than for defect-free specimens.

Based on the results of the analysis of AE-data flow parameters – AE-activity and values of AE pulse amplitudes, as well as based on the results of spectral analysis of AE signals, it is possible to define a list of descriptive AE-parameters, by the values of which it is possible to determine the presence of diffusion layers in dissimilar welded joints. Since the presence of diffusion layers can be detected by local increase of AE-activity and values of amplitudes of AE pulses at a stress of 290–310 MPa, informative from the point of view of identification of the presence of diffusion layers are the parameters plotted as a ratio of local values of AE-parameters at stress in the region of 300 MPa and average values in the region of elastic deformation.

CONCLUSION

As a result of data analysis it was found that for correct data interpretation it is necessary to analyze AE-parameters (AE-activity and values of AE pulse amplitudes) depending on the value of mechanical stress. This way of information presentation reveals the peculiarities of AE data associated with the presence of diffusion layers in the structure of heterogeneous welded joint. It is established that the presence of diffusion layers is manifested by local increase of AE-activity and values of amplitudes of AE pulses at a stress of about 300 MPa, corresponding to the strength limit of the ferrite phase.

For the samples that have undergone long-term heat treatment (exposure at 650°C for 25 h), with the thickness of ferrite interlayer of about 600 μm, lower values of AE activity are registered at the strain hardening section than for samples with smaller interlayer thicknesses, and the values of AE pulse amplitudes are 10–15 dB higher than in previous cases. Such a change in the character of AE data can be explained by structural changes in steel 20 at long high-temperature exposure. After such heat treatment, steel 20 became more ductile, which is confirmed by large values of the ultimate uniform strain and strain to failure of the welded specimen, due to which there was a decrease in the level of AE activity. Also, as a result of long-term heat treatment there was an increase in the average grain size of ferrite in the base metal structure, which led to an increase in the amplitudes of AE pulses.

The growth of AE-activity and the level of amplitudes of AE pulses at a voltage close to the strength limit of the ferrite phase for samples that have undergone long-term heat treatment is not as pronounced as for samples with diffusion interlayers of smaller thickness. Presumably, this may be due to a decrease in the effect of contact hardening of the soft interlayer due to an increase in the width of the ferrite interlayer in the samples after prolonged heat treatment.

Based on the analysis of AE-signals it was found that the presence of diffusion interlayers in the structure of dissimilar welded joints can also be detected by spectral features: the value of the median frequency and spectral entropy. Spectral parameters on samples of specimens with defects are characterized by large values in comparison with defect-free samples.

The research was supported by the Russian Science Foundation grant No. 23-29-00657, https://rscf.ru/project/23-29-00657/.

REFERENCES

1. *Khodakov V.D.*, *Khodakov D.V.* Structure and mechanism of formation of dissimilar welded joints in nuclear power plant made of austenitic and pearlitic steels // Welding International. 2016. Vol. 30. No. 12. Pp. 935–940.
2. *Goncharov A.L.*, *Marchenkov A.Yu.*, *Terentyev E.V.*, *Zhmurko I.E.*, *Sliva A.P.* Study of structural non homogeneity impact on mechanical properties of dissimilar weld joints of carbon steel 20 and corrosion resistant austenitic 12Kh18N10T steel // IOP Conference Series: Materials Science and Engineering. 2019. Vol. 681. No. 012016.
3. *Berezovsky A.V.*, *Votinova E.B.*, *Smolentsev A.S.* The technology of arc welding of dissimilar steels // Diagnostics, Resource and Mechanics of materials and structures. 2023. Is. 5. Pp. 31–38.
4. *Galtsow I.A.*, *Lukin K.I.* Problems and methods of optimization of clad steel welding // Science Almanac. 2020. No. 10–2 (72). Pp. 56–61. (In Russ.)
5. *Shmorgun V.G.*, *Slautin O.V.*, *Evstropov D.A.*, *Taube O.A.* Diffusion Processes on Interlayer Boundary of Explosive-Welded-Ply Composite of System of Cu-Ti // Powder Metallurgy and Functional Coatings. 2014. No. 4. Pp. 36–39. (In Russ.)
6. *Shmorgun V.G.*, *Bogdanov A.I.*, *Kulevich V.P.*, *Razuvaev M.A.*, *Kamalov E.R.* Diffusion Processes In Titanium-Alloy Cr20Ni80 Bimetal // Izvestia Volgograd State Technical University. 2023. No. 2 (273). Pp. 7–11. (In Russ.)
7. *Shmorgun V.G., Bogdanov A.I., Kulevich V.P., Razuvaev M.A., Kamalov E.R.* Diffusion Processes In Titanium-Alloy Cr20Ni80 Bimetal // Izvestia Volgograd State Technical University. 2023. No. 2 (273). Pp. 7–11. (In Russ.)
8. *Ozolin A.V., Burym T.A.* Investigation Of The Interaction Of Metall Matrices Of The Sn-Cu-Co And Sn-Cu-Co-W Systems With Steel Substrates // Computer-Aided Design In Mechanical Engineering. 2022. No. 12. Pp. 21–24. (In Russ.)

9. *Rathod D.W., Pandey S., Singh P.K., Prasad R.* Experimental analysis of dissimilar metal weld joint: Ferritic to austenitic stainless steel // Materials Science and Engineering: A. 2015. Vol. 639. Pp. 259—268.
10. *Matyunin V.M., Goncharov A.L., Marchenkov A.Yu., Zhgut D.A., Abuseyf N., Bobodzhanov A., Lunin V.P.* The Mechanical Properties Control Of Dissimilar Steels Welded Joints From Different Structural Classes // Welding Production. 2020. No. 8. Pp. 7—12. (In Russ.)
11. *Meysam Akbari, Mehdi Ahmadi.* The application of acoustic emission technique to plastic deformation of low carbon steel // Physics Procedia. 2010. Vol. 3. Is. 1. Pp. 795—801.
12. *Higgens F., Carpenter S.* Sources of acoustic emission generated during the tensile deformation of pure iron // Acta Metallurgica. 1978. Vol. 26. Is. 1. Pp. 133—139.
13. *Morrish A.* The Physical Principles of Magnetism. The Institute of Electrical and Electronics Engineers, Inc. 2001. 680 p.
14. *Lord Arthur E.* 6 — Acoustic Emission. Physical Acoustics. Academic Press, 1975. Vol. 11. Pp. 289—353.
15. *Heiple C.R., Carpenter S.H.* Acoustic emission produced by deformation of metals and alloys Part II. Journal of Acoustic Emission. 1987. Vol. 6. No. 4. Pp. 215—237.
16. *Bakshi O.A., Shron R.Z.* Static tensile strength of welded joints with a soft interlayer // Welding Production. 1962. No. 5. Pp. 6—10.
17. *Vinogradov A., Yasnikov I.S., Merson D.L.* Phenomenological approach towards modelling the acoustic emission due to plastic deformation in metals // Scripta Materialia. 2019. Vol. 170.